Transient Stability Analysis of Grid-connected Converters in Wind Turbine Systems Based on Linear Lyapunov Function and Reverse-time Trajectory

Mohammad Kazem Bakhshizadeh, Sujay Ghosh, Guangya Yang, and Łukasz Kocewiak

Abstract—**As the proportion of converter-interfaced renewable energy resources in the power system is increasing, the strength of the power grid at the connection point of wind turbine generators (WTGs) is gradually weakening. Existing research has shown that when connected with the weak grid, the stability of the traditional grid-following controlled converters will deteriorate, and unstable phenomena such as oscillation are prone to arise. Due to the limitations of linear analysis that cannot sufficiently capture the stability phenomena, transient stability must be investigated. So far, standalone time-domain simulations or analytical Lyapunov stability criteria have been used to investigate transient stability. However, the time-domain simulations have proven to be computationally too heavy, while analytical methods are difficult to formulate for larger systems, require many modelling assumptions, and are often conservative in estimating the stability boundary. This paper proposes and demonstrates an innovative approach to estimating the transient stability boundary via combining the linear Lyapunov function and the reverse-time trajectory technique. The proposed methodology eliminates the need of time-consuming simulations and the conservative nature of Lyapunov functions. This study brings out the clear distinction between the stability boundaries with different post-fault active current ramp rate controls. At the same time, it provides a new perspective on critical clearing time for wind turbine systems. The stability boundary is verified using time-domain simulation studies.**

Index Terms—**Lyapunov direct method, non-autonomous systems, phase-locked loop (PLL), time trajectory reversal, transient stability assessment, wind turbine converter system.**

I. Introduction

As of 2021, the worldwide installation of wind power capacity has reached approximately 743 GW, contributing significantly to a reduction of over 1.1 billion tonnes of CO_2 emissions globally [1]. The wind industry is poised for continued growth due to technological innovations, economies of scale, and policy support worldwide. However, the increasing proportion of converter-interfaced renewable energy resources in the power system [2] has weakened the connection strength between wind turbine generators (WTGs) and the power grid. Previous research has demonstrated that the dynamic characteristics of traditional grid-following controlled converters can deteriorate when connected to a weak grid, leading to unstable phenomena such as oscillation [3], [4].

Traditionally, the stability of wind farm connections has been analyzed using linearized model-based approaches such as eigenvalue analysis [5], [6] or impedance-based stability analysis [7], [8]. These methods assume that the system, including the wind turbine (WT) and the connected power system, behaves linearly under small disturbances and that stability is only analyzed within the vicinity of operating points. However, it has been noted in [9] that small-signal stability assessment alone cannot guarantee overall stability. Therefore, transient stability must also be investigated to ensure that the system remains stable under larger disturbances.

In [10], it has been demonstrated that large disturbances can destabilize the phase-locked loop (PLL), which can have a significant impact on the transient stability of the WT system. In general, transient stability has been evaluated through time-domain simulations. Time-domain simulation is simple but cannot provide a closed-form solution for quantifying stability margins. Therefore, it is necessary to repeat the simulations over a large set of system conditions (like phase portraits) to identify the system boundary, i.e., the region of attraction (RoA) [11].

Alternatively, analytical transient stability methods such as equal area criteria and Lyapunov direct method [12] provide a closed-form solution for the system. Here, a non-linear Lyapunov function (LF) is constructed such that after a disturbance, the decrease in energy results in a stable system. A classical non-linear LF is constructed for synchronous generators based on its swing equation [13]. Efforts have been made to extend the same to WT systems [14]; however, the system is assumed to have autonomous behaviour, as shown in Section III of [14]. In [15], a non-linear LF for a WT

Manuscript received: March 23, 2023; revised: June 23, 2023; accepted: September 6, 2023. Date of CrossCheck: September 6, 2023. Date of online publication: November 13, 2023.

M. K. Bakhshizadeh, S. Ghosh (corresponding author), and Ł. Kocewiak are with Ørsted Wind Power A/S, Nesa Allé 1, 2820, Denmark (e-mail: modow@orsted.com; sujgh@orsted.com; lukko@orsted.com).

G. Yang is with the Technical University of Denmark, Anker Engelunds Vej 1, 2800, Denmark (e-mail: gyy@elektro.dtu.dk).

DOI: 10.35833/MPCE.2023.000190

with non-autonomous behaviour is constructed based on [16], which states that a system has a smaller RoA when the post-fault active current ramp is higher. However, the approach to constructing the LF is highly complex and results in a conservative estimate of the RoA.

Recent developments have focused on maximizing the system's RoA by formulating an optimization problem using sum-of-squares programming [17]. Additionally, some machine learning (ML) techniques [18] have been studied to achieve a better estimate of the RoA. However, these techniques require significant expertise in data-driven techniques. Considering the high computation burden of repeated time-domain simulations over a large set of system conditions, the mathematical complexities of non-linear analytical methods coupled with a conservative estimate of system's RoA, and the requirement of domain expertise in data-driven techniques for optimization and ML techniques, the objective of this paper is to propose a fast and simplified transient stability assessment method that the industry can easily adopt.

This paper presents a novel approach to transient stability assessment of grid-connected converters in WT systems by combining the advantages of time-domain simulations and analytical (Lyapunov) stability methods. Specifically, we use the reverse-time trajectory technique in conjunction with linear LFs to estimate the system boundary. Compared with non-linear LFs, constructing linear LFs is simple and has an established procedure. Additionally, the reverse-time trajectory only needs to be performed for stable cases, significantly reducing the number of repeated time-domain simulations.

The reverse-time trajectory has been the subject of extensive research for several decades [19]-[21]. The application of reverse-time trajectory in dynamic systems dates back to 1915 when it was initially used to analyze a three-body problem [22]. Subsequently, the reverse-time trajectory has been employed in various problems related to thermodynamics and quantum mechanics [23]-[25]. Reference [26] provides an extensive overview of reverse-time dynamics, including system equations and conservative and dissipative behaviour. Built on our previous research on non-linear modelling and transient stability assessment of WTs [9], [15], [27], [28], our proposed methodology aims to provide a fast, simple, and practical solution for industry without requiring complex mathematical analysis. The following is the contribution in the paper.

1) A hybrid approach to estimating the post-fault system boundary (i.e., RoA) is proposed based on linear LF and reverse-time trajectory.

2) This work brings out the clear distinction between the system boundaries with different post-fault active current ramp rate controls.

3) A new perspective on critical clearing time for WT systems is discussed.

The remainder of this paper is organized as follows. Section II provides an overview of the mathematical preliminaries for the proposed transient stability assessment approach. Section III details the large signal reduced-order WT model and its transient stability assessment. The time-domain validation of the proposed approach is presented in Section IV. The paper concludes with Section V.

II. Mathematical Preliminaries for Proposed Transient Stability Assessment Approach

Most of the dynamical systems can be described by the following ordinary differential equation (ODE):

$$\dot{\boldsymbol{x}}=\boldsymbol{f}(t,\boldsymbol{x},\boldsymbol{u}) \tag{1}$$

where $\boldsymbol{x}\in\mathbb{R}^n$ is the vector of state variables of the system; $\dot{\boldsymbol{x}}$ is the time derivative of vector $\boldsymbol{x}$; t is the time; and $\boldsymbol{u}\in\mathbb{R}^m$ is the vector of input signals. Usually, the inputs are defined based on time and state variables; therefore, they can be omitted from (1). If $\boldsymbol{f}$ is not an explicit function of time, then the system defined by (2) is called an autonomous system [29].

$$\dot{\boldsymbol{x}}=\boldsymbol{f}(\boldsymbol{x}) \tag{2}$$

An equilibrium point for a dynamical system is defined as a point $\tilde{\boldsymbol{x}}$, for which $\boldsymbol{f}(\tilde{\boldsymbol{x}})=\boldsymbol{0}$. In other words, if the system solution $\boldsymbol{x}(t)$ reaches $\tilde{\boldsymbol{x}}$, it stays there forever.

A. Lyapunov Direct Method for Stability Analysis

A scalar continuous and differentiable function V: $\mathbb{D}\subset\mathbb{R}^n\rightarrow\mathbb{R}$ is called an LF for the system (2) with $\boldsymbol{x}=\boldsymbol{0}$ such that (3)-(5) are satisfied, which also shows that the system is stable.

$$V(\boldsymbol{0}^n)=0\Leftrightarrow\boldsymbol{x}=\boldsymbol{0}^n \tag{3}$$

$$V(\boldsymbol{x})>0\quad\forall\boldsymbol{x}\in\mathbb{D}-\{\boldsymbol{0}^n\} \tag{4}$$

$$\dot{V}(\boldsymbol{x})\leq 0\quad\forall\boldsymbol{x}\in\mathbb{D} \tag{5}$$

Furthermore, if $\dot{V}(\boldsymbol{x})<0, \forall\boldsymbol{x}\in\mathbb{D}-\{\boldsymbol{0}^n\}$, then the system is asymptotically stable, i.e., $\lim\limits_{t\rightarrow\infty}\boldsymbol{x}(t)=\boldsymbol{0}^n$. It must be noted that if the equilibrium point $\tilde{\boldsymbol{x}}$ is not the origin, it can be shifted by a change of variables.

B. RoA for Dynamical Systems

The RoA for an equilibrium point is defined as a set:

$$\mathbb{D}=\left\{\boldsymbol{x}_{init}\in\mathbb{R}^n\text{: }\lim_{t\rightarrow\infty}\boldsymbol{\varphi}(t,\boldsymbol{x}_{init})=\boldsymbol{0}^n\right\} \tag{6}$$

where $\boldsymbol{x}_{init}$ denote the initial state variables of a dynamical system; and $\boldsymbol{\varphi}(t,\boldsymbol{x}_{init})$ denotes the dynamical system for a specific initial condition.

Finding the exact RoA is a highly complex task; instead, finding an inner estimate of the exact RoA is common practice. A set defined by $V(\boldsymbol{x})\leq c$ $(c>0)$ is called a sublevel set of the LF $V(\boldsymbol{x})$, which is a set that if the solution trajectory $\boldsymbol{x}(t)$ enters, then it cannot exit. Therefore, there exists

$$V(\boldsymbol{x})\leq c\subset\mathbb{D} \tag{7}$$

In other words, obtaining the biggest estimate of the RoA is to find appropriate LFs and then maximize c.

For example, the RoA of the reversed Van der Pol system (8) is presented in Fig. 1, where it is evident that if the initial point is inside the RoA, the system is attracted to the origin (green trajectory), while an initial point outside the RoA does not converge to the origin (red trajectory), meaning such trajectories are unstable.

$$\begin{cases} \dot{x}_1 = -x_2 \\ \dot{x}_2 = x_1 - x_2(1 - x_1^2) \end{cases} \tag{8}$$

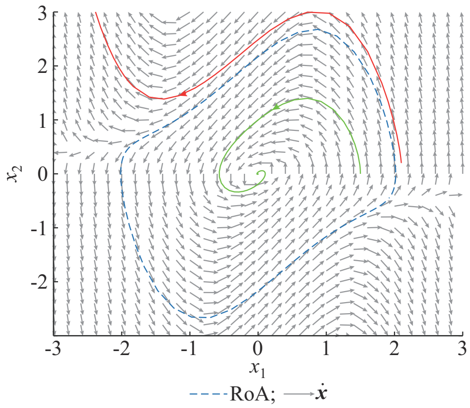

Fig. 1. RoA of reversed Van der Pol system (8).

C. LF Candidate from Linearized System

The non-linear dynamical system (2) can be approximated by a linear model in a small region around the operating point (i.e., origin) by small-signal linearization as:

$$\Delta \boldsymbol{x} = \boldsymbol{A} \Delta \boldsymbol{x} \tag{9}$$

where $\boldsymbol{A} = \left.\dfrac{\partial \boldsymbol{f}}{\partial \boldsymbol{x}}\right|_{\boldsymbol{x} = \boldsymbol{0}^n}$.

If $\boldsymbol{A}$ is a Hurwitz matrix, then a quadratic LF $V(\boldsymbol{x})$ can easily be found by using the linearized model (9) as:

$$V(\boldsymbol{x}) = \boldsymbol{x}^{\mathrm{T}} \boldsymbol{P} \boldsymbol{x} \tag{10}$$

where for any positive-definite matrix $\boldsymbol{Q} \succ \boldsymbol{0}$, positive-definite matrix $\boldsymbol{P} \succ \boldsymbol{0}$ is the solution of the Lyapunov equation, and

$$\boldsymbol{P}\boldsymbol{A} + \boldsymbol{A}^{\mathrm{T}} \boldsymbol{P} + \boldsymbol{Q} = \boldsymbol{0} \tag{11}$$

For example, for the reversed Van der Pol system (8), the linearization around the origin results in:

$$\boldsymbol{A} = \begin{bmatrix} 0 & -1 \\ 1 & -1 \end{bmatrix} \tag{12}$$

By assuming $\boldsymbol{Q} = \begin{bmatrix} 1 & -0.5 \\ -0.5 & 1 \end{bmatrix} \succ \boldsymbol{0}$ and solving the Lyapunov equation in (11), we have:

$$\boldsymbol{P} = \begin{bmatrix} 1 & -0.5 \\ -0.5 & 1 \end{bmatrix} \tag{13}$$

The computed matrix $\boldsymbol{P}$ results in the LF (14), whose maximum estimated RoA is presented in Fig. 2. For the LF to be valid, the time derivative should be negative, which is also highlighted. Figure 2 shows that not only $\dot{V}(\boldsymbol{x})$ should be negative, but also $V(\boldsymbol{x}) \le c$ is essential.

$$V(x_1, x_2) = [x_1 \quad x_2] \boldsymbol{P} \begin{bmatrix} x_1 \\ x_2 \end{bmatrix} = x_1^2 - x_1 x_2 + x_2^2 \tag{14}$$

D. Dynamical Systems as Mappings

A dynamical system can be considered a function that maps the initial conditions to the final conditions after a specific time. The following definitions give some of the main properties related to the dynamical system stability [29]-[31].

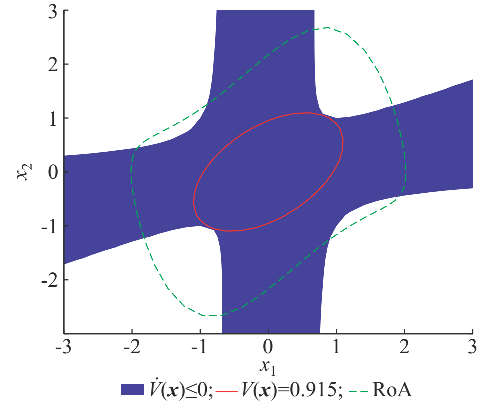

Fig. 2. Estimated RoA of reversed Van der Pol system by LF (14).

Definition 1 Uniqueness of the solution of a dynamical system: a sufficient condition for the uniqueness of the solution is that the function $\boldsymbol{f}$ should be locally Lipschitz, i.e., it is a continuous function, and its derivative with respect to the state variables is bounded [29].

$$\left\| \boldsymbol{f}(t, \boldsymbol{x}) - \boldsymbol{f}(t, \boldsymbol{y}) \right\| \le L \left\| \boldsymbol{x} - \boldsymbol{y} \right\| \tag{15}$$

where L denotes a constant.

It should be noted that this is a weaker condition than the differentiability of the function $\boldsymbol{f}$.

Definition 2 Boundary preservation in a homeomorphic mapping: the continuous function $\boldsymbol{f}: \boldsymbol{X} \rightarrow \boldsymbol{Y}$ is homeomorphic [30] if it is bijective and its inverse is also continuous, such that (16) is satisfied, which means that if $\boldsymbol{f}$ is homeomorphic from set $\boldsymbol{X}$ to set $\boldsymbol{Y}$ and if $\mathbb{A}$ is a subset of $\boldsymbol{X}$, then the image of the boundary of $\mathbb{A}$ is equal to the boundary of the image of $\mathbb{A}$.

$$\boldsymbol{f}(\partial \mathbb{A}) = \partial(\boldsymbol{f}(\mathbb{A})) \quad \forall \mathbb{A} \subseteq \boldsymbol{X} \tag{16}$$

where $\partial \mathbb{A}$ denotes the boundary of a space $\mathbb{A}$.

Definition 3 Reverse-time trajectory: if $\boldsymbol{f}$ is a Lipschitz function, a unique solution trajectory for each initial condition is guaranteed. Moreover, if the differential equations are solved backwards in time, the same unique trajectory is traversed [31]. This means that $\boldsymbol{F}(\boldsymbol{x}) = \boldsymbol{\varphi}(T, \boldsymbol{x})$, where $\boldsymbol{F}$ is an invertible function, and T is a defined time. Therefore, the response of a dynamical system after a given time for initial conditions chosen from a closed set in $\mathbb{B} \subset \mathbb{R}^n$ will lie in a closed set $\mathbb{D} \subset \mathbb{R}^n$ such that

$$\partial \mathbb{D} = \partial(\boldsymbol{F}(\mathbb{B})) = \boldsymbol{F}(\partial \mathbb{B}) \tag{17}$$

This is quite a useful conclusion which means that simulating a dynamical system numerically for a boundary of initial conditions can give the boundary of the final states, and it is guaranteed that for any initial point inside this boundary, the final response lies in the calculated final boundary.

E. Estimating RoA from Reverse-time Trajectory

The reverse-time trajectory technique uses a simulation method to extend an initial estimate of the RoA. It draws its name from reversing the direction of the trajectories by backward integration. This is equivalent to forward integration of the system, as shown in (18), which is obtained from (2) by replacing t with $-t$.

$$\dot{\boldsymbol{x}} = -\boldsymbol{f}(\boldsymbol{x}) \tag{18}$$

System (18) has the same trajectory configuration in the state space as system (2), but with reversed arrowheads on the trajectories [29], [32]. The initial value for (18) is computed from the linear LF discussed in Section II-C.

Suppose the initial point selected is in close proximity to the stable equilibrium point. In that case, the uniqueness of the solution guarantees that all points in the reversed-time trajectory will be attracted to the equilibrium point. Additionally, suppose the stable equilibrium point is bounded by a limit cycle. In that case, the limit cycle can be identified by reversing the trajectory, but this may require a longer simulation time, as demonstrated in Fig. 3.

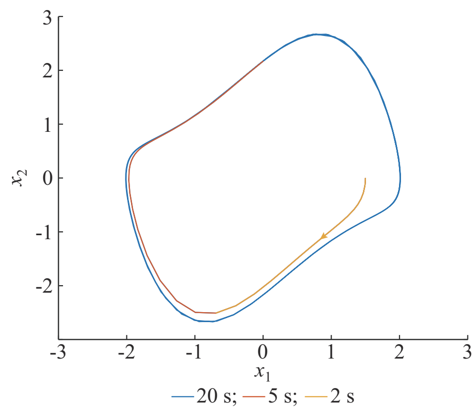

Fig. 3. Reverse-time trajectory for reversed Van der Pol system (8).

In a conventional RoA, any trajectory inside the region will eventually reach the equilibrium point, but does not provide any information regarding the time to reach the equilibrium, i. e., it could take a few seconds to several minutes. However, in power system stability, time is an important factor, and it is often required that the system reaches a steady state within a specific time frame, known as the settling time [33]. Therefore, in this paper, we introduce a time-limited region of attraction (TLRoA), which is a subset of the RoA such that any trajectory on its boundary will reach the equilibrium at the same time, and any trajectory inside will reach the equilibrium in less than the said time.

To estimate the TLRoA after a disturbance, the differential equations of the system are solved backwards until the disturbance, assuming a tolerance band (e.g., ±5%) around the equilibrium point. It is crucial that the tolerance band must be a RoA. Therefore, a small RoA around the equilibrium point is first identified using linearized analysis. Then, the mapping theory explained in this subsection is used to transform this region into another region through the backward solution of the original ODEs, as shown in Fig. 4, where pink region is the initial RoA obtained from linear LF, and the purple region is the final RoA obtained from reverse-time trajectory (black lines) with the initial conditions (red dots).

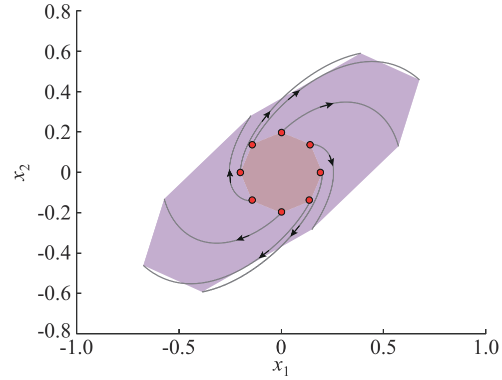

Fig. 4. Mapping initial states to final states by backward solution of ODEs for reversed Van der Pol system (8).

III. Large Signal Reduced-order WT Model and Its Transient Stability Assessment

Our previous works [15], [27], [28] have demonstrated that a type-4 WT can be simplified to a grid-side converter with a constant DC voltage during grid faults, as shown in Fig. 5(a), resulting in a current-controlled source, as shown in Fig. 5(b), with reference values obtained from the grid codes. For large-signal stability analysis, the fast inner current control dynamics can be neglected, and the impact of the shunt capacitor filter on stability can be disregarded if the current is controlled on the grid-side LCL filter. A reduced-order WT model in the dq domain is presented in Fig. 5(c), with synchronous reference frame (SRF) PLL for synchronisation. The detailed descriptions of variables in Fig. 5 can be found in [28].

The equivalent swing equation of the WT converter system derived in [28] can be presented as:

$$M_{eq}\ddot{\delta} = T_{m_{eq}} - T_{e_{eq}} - D_{eq}\dot{\delta} \tag{19}$$

$$\begin{cases} M_{eq} = 1 - k_p L_g i_d^c \\ T_{m_{eq}} = k_p \left(\overset{\cdot}{\overline{r_{Lg} i_q^c}} + \overset{\cdot\cdot}{\overline{L_g i_q^c}} + \overset{\cdot}{\overline{L_g i_d^c}}\, \omega_g \right) + k_i \left(r_{Lg} i_q^c + \overset{\cdot}{\overline{L_g i_q^c}} + L_g i_d^c \omega_g \right) \\ T_{e_{eq}} = (k_i V_g \sin\delta + k_p \dot{V}_g \sin\delta) + M\dot{\omega}_g \\ D_{eq} = k_p \left(V_g \cos\delta - \overset{\cdot}{\overline{L_g i_d^c}} \right) - k_i L_g i_d^c \end{cases} \tag{20}$$

where M_{eq} is the equivalent inertia; i_d^c and i_q^c are the pre-disturbance active and reactive currents, respectively; $T_{m_{eq}}$ is the equivalent mechanical torque; $T_{e_{eq}}$ is the equivalent electrical torque; D_{eq} is the equivalent damping; δ is the PLL angle; k_p and k_i are the PLL controller gains; r_{Lg} and L_g are the grid-side resistance and reactance, respectively; and V_g and ω_g are the grid voltage and frequency, respectively.

Equation (19) represents a second-order non-linear damped differential equation that is used to model the WT system. This equation considers the time-varying nature of the system parameters, represented by the derivatives in (20). The WT system is modelled in a dq frame, rotating at a fixed frequency ω_0.

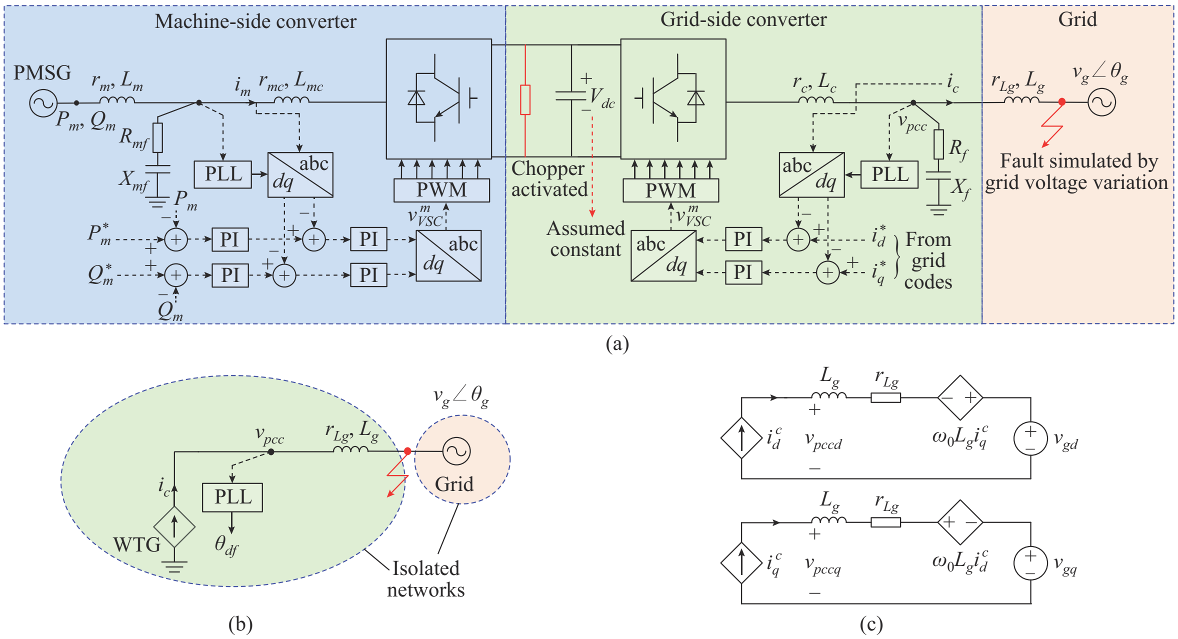

Fig. 5. WT model. (a) Full topology of type-4 WT system, highlighting actions/assumptions during faults. (b) Reduced-order model (ROM) of type-4 WT considering actions/assumptions, showing synchronization instability of WT systems during grid faults as well. (c) System representation of ROM in dq domain.

Table I presents the system and control parameters of the WT converter system considered in this study, where the PLL controller gains are chosen to obtain an oscillatory PLL behaviour; and *SCR* denotes the short circuit ratio.

TABLE I
SYSTEM AND CONTROL PARAMETERS [34]

Parameter	Value
Rated power S_b	12 MVA
Nominal grid voltage V_g	$690\sqrt{2/3}$ V
Rated frequency f_g	50 Hz
Grid-side resistance and reactance r_{Lg}, L_g	0.0018 Ω, 1.0608×10^{-4} H (*SCR*=1.2, *X*/*R*=18.6)
Pre-disturbance active and reactive currents i_d^c, i_q^c	1.0 p.u., 0 p.u.
PLL controller gains k_p, k_i	0.025, 1.5
Post-fault active current ramp rate $i_d^{c,ramp}$	28.4 kA/s or 42.6 kA/s

A. Estimating TLRoA

1) LF Candidate from Linearized System

The first step in estimating the WT system boundary is obtaining an initial RoA, which is carried out by constructing a LF from the linearized equations of the WT system (18). In [15], the system (18) was linearized around $\boldsymbol{x}$, which can be expressed as:

$$\boldsymbol{A}=\left.\frac{\partial \boldsymbol{f}}{\partial \boldsymbol{x}}\right|_{\boldsymbol{x}=\tilde{\boldsymbol{x}}}=\begin{bmatrix} 0 & 1 \\ \dfrac{\mp k_i V_g}{1-k_p L_g i_d^c}\sqrt{1-\gamma^2} & \dfrac{k_i L_g i_d^c \mp k_p V_g\sqrt{1-\gamma^2}}{1-k_p L_g i_d^c} \end{bmatrix} \tag{21}$$

where the detailed description of γ can be found from [15].

By assuming $\boldsymbol{Q}$ as an identity matrix, $\boldsymbol{P}$ can be computed from (11). Further, the LF constructed from the linear WT system is presented in (22). The RoA estimated by linearized model (19) with a selected energy level of 0.001 is illustrated in Fig. 6. It must be noted that for simplicity, in Fig. 6, the equilibrium point is shifted to the origin.

$$V(\boldsymbol{x})=ax_1^2+bx_1x_2+cx_2^2 \tag{22}$$

where $a=49.66$; $b=0.0026$; and $c=0.129$.

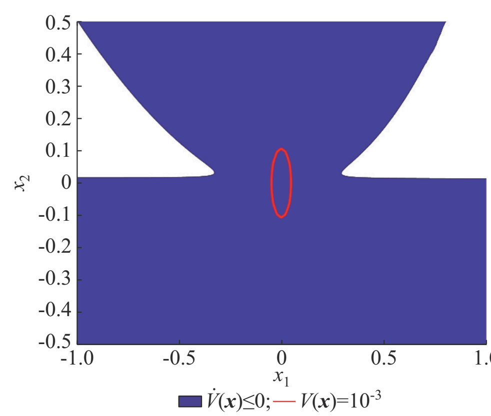

Fig. 6. RoA estimated by linearized model (19) with equilibrium point hifted to origin.

2) Backward Solution and Reverse-time Trajectory

To estimate the TLRoA, the system (19) can be solved backwards in time using the initial conditions obtained from the initial RoA boundary, which was determined in Fig. 6. For this study, the system was solved backwards for 2.25 s, which is the time for the oscillations to dampen out. After this period, the system was further solved backwards until the post-fault active current was ramped down to the fault-clearing time. The estimated TLRoA with a post-fault active current ramp rate of 28.4 kA/s, as given in (18), is shown in Fig. 7, where the black arrows represent the reverse time trajectory directions; and the red dots are the final solutions of all initial conditions chosen from the boundary of (22). The set of red dots represent the TLRoA. Unlike RoA, for TLRoA, all the points at the boundary reach the equilibrium point at the same time; therefore, the enclosed TLRoA is a subset of the actual RoA.

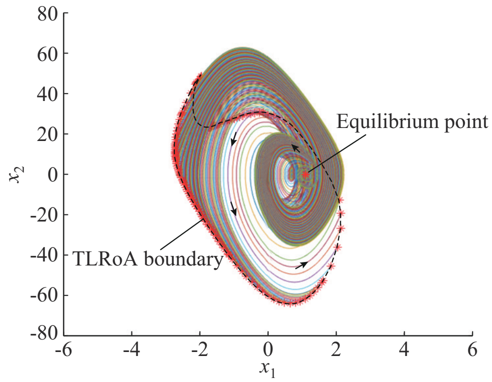

Fig. 7. Estimated TLRoA with a post-fault active current ramp rate of 28.4 kA/s.

To generate the smooth TLRoA in Fig. 7, the number of samples (initial conditions) is $N=186$. For a similar system, generating the actual RoA through forward simulations requires $N=3213$ [27]. This brings out the advantage of our proposed approach. One must ensure that enough samples are taken from the boundary of the initial RoA to have a smooth boundary for the set of final conditions. This limitation is a known issue in numerical computations, and there are adaptive sampling techniques to reduce the step size when there are large variations in a function. The methodology for choosing the sampling rate is not the focus of this paper and will be addressed through future publications.

B. Transient Stability Assessment Methodology

The primary question in assessing transient stability is whether a power system can return to equilibrium following a disturbance. To address this, a hybrid approach is proposed, where the estimated TLRoA represents the post-disturbance system, and a forward time-domain simulation is carried out to observe the system behaviour during the disturbance. Figure 8 shows the simulation results of a balanced fault (severe grid voltage dip) for an extended period with $V_g=0$ p.u., $i_d^c=0.01$ p.u., and $i_q^c=-1$ p.u., where (x,y) coordinates of the triangle, square, and pentagon are taken from Fig. 9 to calculate the corresponding clearing time ct highlighted in red. $ct_{28.4\,\mathrm{kA/s}}$ is the clearing time with the post-fault active current ramp rate of 28.4 kA/s; and $ct^1_{42.6\,\mathrm{kA/s}}$ and $ct^2_{42.6\,\mathrm{kA/s}}$ are the clearing time with the post-fault active current ramp rate of 42.6 kA/s. As pointed out in [28], there will be PLL angle and frequency jumps after the fault is cleared. Therefore, an additional curve (red) is calculated in Fig. 8 that depicts the PLL angle and frequency with the jumps when the fault is cleared at that time.

Based on Section III-A, Fig. 9 presents the estimated TLRoA for the system (18) with two different post-fault active current ramp rates, 28.4 kA/s and 42.6 kA/s. As expected, the system with a faster ramp rate has a smaller TLRoA [15]. Additionally, the red curve from Fig. 8 is overlaid on the estimated TLRoA in Fig. 9 in x_1-x_2 coordinates, with the PLL angle reset to π when it reaches $-\pi$. This is to eliminate the illustration of neighbouring RoAs for equilibrium points that repeat every 2π.

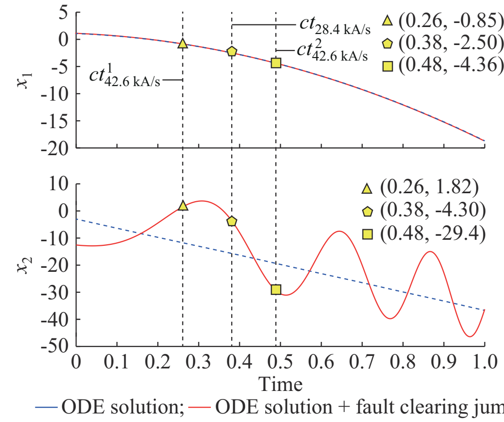

Fig. 8. Forward solution of system during severe fault with $V_g=0$ p.u., $i_q^c=0.01$ p.u., and $i_q^c=-1$ p.u..

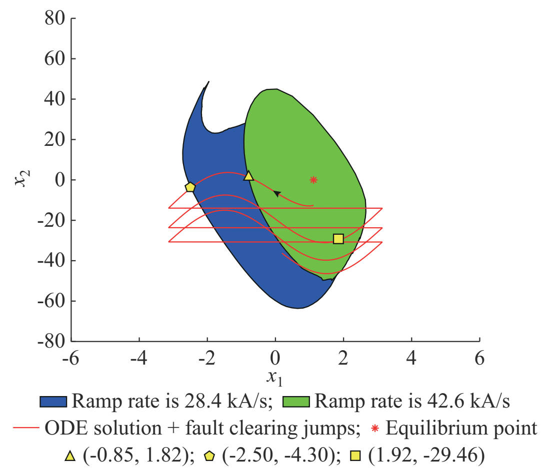

Fig. 9. Estimated TLRoA for system (18) with two different post-fault active current ramp rates.

For assessing transient stability, it is proposed that clearing the fault at any point along the fault trajectory (red line in Fig. 9) inside the TLRoA will guarantee the system's attraction to its post-fault equilibrium point. For instance, if the fault is cleared before reaching the yellow triangle in Fig. 9, then both systems with post-fault active current ramp rates of 28.4 kA/s and 42.6 kA/s will be stable. If the fault persists beyond the yellow triangle (but not beyond the yellow pentagon), then only the system with a post-fault active current ramp rate of 28.4 kA/s will be stable. Similarly, if the fault persists beyond the yellow pentagon (but not beyond $-\pi$), then both systems will become unstable. Moreover, if the fault persists until the yellow square, both systems will be stable again. Thus, it is observed that the fault trajectory exits and re-enters the TLRoA multiple times, suggesting that the WT system can be stable if the fault is cleared at a later time, indicating the WT system has multiple critical clearing time.

The time at which the fault trajectory reaches the critical points, indicated by the yellow triangle and yellow pentagon, can be read off from Fig. 8, with the horizontal axis showing the clearing time. The clearing time and the resulting system stability will be verified using actual EMT WT models. While the primary focus in this work is on individual WTs, it must be noted that our proposed approach has the potential for adaptability at the wind power plant (WPP) level as well. The same approach can be adapted by aggregating the full WPP with multiple WTs as a single machine equivalent, as explored in [35].

IV. Time-domain Verification

This section evaluates the proposed approach through time-domain simulations using an EMT WT switching model in PSCAD. The model is designed based on the configuration described in [28], where the current controller gains are adjusted to achieve a fast response. A complete fault ride-through is simulated. When a symmetrical fault occurs (the grid voltage is stepped down to 0%), the reactive current is stepped up to −1 p.u., and the active current is stepped down to 0.01 p.u.. When the fault is cleared (the voltage is stepped up back to 1 p.u.), the reactive current is set to be the pre-fault value of 0 p.u.; however, the active current is ramped up (e.g., 28.4 kA/s), not to stress the mechanical structure. The mathematical model for the WT system during and after the fault is discussed in detail in [28].

Two case studies for the WT system with two different post-fault active current ramp rates are carried out in PSCAD to investigate and cross-check the theoretical critical clearing time obtained from Fig. 8.

Figure 10 shows the time-domain simulations indicating the clearing time for the WT system with a post-fault active current ramp rate of 28.4 kA/s. The system is unstable when the fault is allowed to propagate beyond 0.37 s and cleared sometime before 0.47 s. However, if the fault is allowed to propagate and cleared at 0.48 s, the system stabilizes. This is in line with the theoretical understanding discussed in Section III-B. It must be noted that, unlike linear systems, nonlinear systems have multiple equilibrium points; in our system, it repeats every (±2π,0). This is why, in Fig. 9, the PLL angle is reset/wrapped to π when it reaches −π. Therefore, during faults, if the fault trajectory is allowed to propagate such that it exits and re-enters its RoA, then the fault is cleared; in such a case, the system is stable. However, the system will be unstable if the fault trajectory is outside the RoA when the fault is cleared. The PSCAD simulations corroborate the analytical conclusions. Similar results have been reported in [36], which was done for grid-forming converters.

Similarly, Fig. 11 shows the time-domain results by PSCAD simulations indicating the clearing time for the WT systems with a post-fault active current ramp rate of 42.6 kA/s. The system is unstable when the fault is allowed to propagate beyond 0.25 s and cleared sometime before 0.47 s. However, if the fault is allowed to propagate and cleared at 0.48 s, the system stabilizes. Again, this is consistent with the theoretical understanding discussed in Section III-B.

Overall, the proposed methodology has a high level of confidence in its application for investigating the transient stability of WTs. The traditional method of estimating the RoA of the post-fault system through forward-time simulation involves guessing initial conditions, resulting in either a stable or an unstable trajectory. In contrast, our proposed methodology only solves stable trajectories in reverse time, resulting in a quicker and more efficient estimation of the RoA.

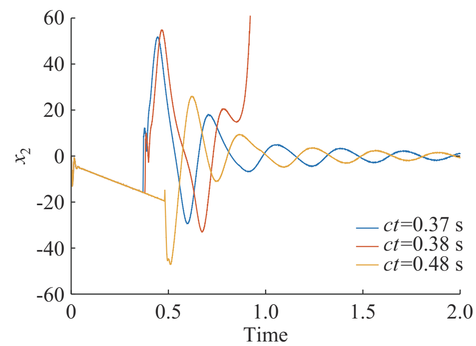

Fig. 10. Verification of identified critical clearing time by PSCAD simulations with post-fault active current ramp rate of 28.4 kA/s.

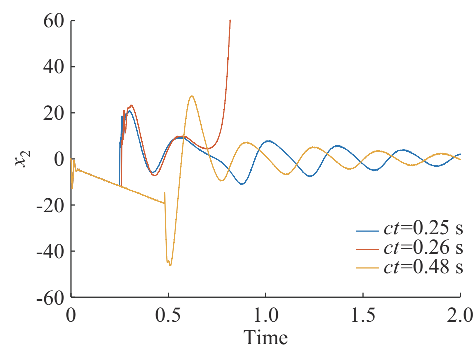

Fig. 11. Clearing time for WT systems with post-fault active current ramp rate of 42.6 kA/s.

While some efforts have been made to analytically estimate the RoA of a WT with non-autonomous behaviour, such as ramps in active current, these methodologies can be complex and conservative. In contrast, our proposed methodology utilizes a simplified analytical LF to estimate the initial conditions for the reverse-time trajectory solutions. As a result, the industry can adopt this methodology without requiring complex mathematical analysis.

Our proposed methodology can enable power system operators and wind farm owners to take advantage of multiple critical clearing time for WT systems. By clearing faults later, uninterrupted supply from the WTs can be achieved, which benefits both parties. This can motivate the development of new power system protection philosophies and smart relays, which can enhance the overall stability and reliability of the power system.

V. Conclusion

This work extends our research on non-linear modelling and transient stability assessment of WT systems. It presents a methodology for transient stability assessment of a WT system with a non-autonomous behaviour.

1) A hybrid approach based on linear LF and reverse-time trajectory provides a good estimate of the post-fault system boundary (i. e., RoA), where it was observed that the clearing time obtained from the proposed approach is consistent with the results obtained from the PSCAD simulations.

2) This work brings out the clear distinction between the system boundaries with different post-fault active current ramp rate controls, i. e., a system with a faster post-fault active current ramp rate has a smaller RoA.

3) A new perspective on critical clearing time for WT systems is discussed, which shows that sometimes a later clearing time helps the system to regain stability, motivating the development of new power system protection philosophies and smart relays, which can enhance the overall stability and reliability of the power system.

While the primary focus in this work is on individual WTs, it must be noted that our proposed approach has the potential for adaptability at the WPP level as well, where the WPP with multiple WTs can be aggregated as an equivalent single machine, and this is a plausible future extension of our research.

References

[1] GWEC. (2021, Mar.). Global wind report 2021. [Online]. Available: http://www.eqmagpro.com/gwec-global-wind-report-2021/

[2] J. Tan and Y. Zhang, "Coordinated control strategy of a battery energy storage system to support a providing multi-timescale frequency ancillary services," *IEEE Transactions on Sustainable Energy*, vol. 8, no. 3, pp. 1140-1153, Jul. 2017.

[3] Y. Huang, X. Yuan, J. Hu *et al*., "Modeling of VSC connected to weak grid for stability analysis of DC-link voltage control," *IEEE Journal of Emerging and Selected Topics in Power Electronics*, vol. 3, no. 4, pp. 1193-1204, Dec. 2015.

[4] C. Zhang, X. Cai, A. Rygg *et al*., "Sequence domain SISO equivalent models of a grid-tied voltage source converter system for small-signal stability analysis," *IEEE Transactions on Energy Conversion*, vol. 33, no. 2, pp. 741-749, Jun. 2018.

[5] J. Hu, Q. Hu, B. Wang *et al*., "Small signal instability of PLL-synchronized type-4 wind turbines connected to high-impedance AC grid during LVRT," *IEEE Transactions on Energy Conversion*, vol. 31, no. 4, pp. 1676-1687, Dec. 2016.

[6] F. Wu, X. Zhang, K. Godfrey *et al*., "Small signal stability analysis and optimal control of a wind turbine with doubly fed induction generator," *IET Generation*, *Transmission & Distribution*, vol. 1, no. 5, p. 751, Aug. 2007.

[7] H. Liu and J. Sun, "Voltage stability and control of offshore wind farms with AC collection and HVDC transmission," *IEEE Journal of Emerging and Selected Topics in Power Electronics*, vol. 2, no. 4, pp. 1181-1189, Dec. 2014.

[8] M. Amin and M. Molinas, "Understanding the origin of oscillatory phenomena observed between wind farms and HVDC systems," *IEEE Journal of Emerging and Selected Topics in Power Electronics*, vol. 5, no. 1, pp. 378-392, Mar. 2017.

[9] S. Ghosh, G. Yang, M. K. B. Dowlatabadi *et al*., "Nonlinear stability analysis of a reduced-order wind turbine VSC-grid model operating in weak grid conditions," in *Proceedings of 20th International Workshop on Large-scale Integration of Wind Power into Power Systems as well as on Transmission Networks for Offshore Wind Power Plants* (*WIW 2021*), Berlin, Germany, Sept. 2021, pp. 457-463.

[10] M. Bravo, A. Garcés, O. D. Montoya *et al*., "Nonlinear analysis for the three-phase PLL: a new look for a classical problem," in *Proceedings of 2018 IEEE 19th Workshop on Control and Modeling for Power Electronics* (*COMPEL*), Padua, Italy, Jun. 2018, pp. 1-6.

[11] S. L. Brunton, B. W. Brunton, J. L. Proctor *et al*., "Koopman invariant subspaces and finite linear representations of nonlinear dynamical systems for control," *PLoS One*, vol. 11, no. 2, p. e0150171, Feb. 2016.

[12] T. L. Vu and K. Turitsyn, "Lyapunov functions family approach to transient stability assessment," *IEEE Transactions on Power Systems*, vol. 31, no. 2, pp. 1269-1277, Mar. 2016.

[13] D. J. Hill, I. A. Hiskens, and I. M. Y. Mareels, "Stability theory of differential/algebraic models of power systems," *Sadhana*, vol. 18, no. 5, pp. 731-747, Sept. 1993.

[14] Z. Tian, Y. Tang, X. Zha *et al*., "Hamilton-based stability criterion and attraction region estimation for grid-tied inverters under large-signal disturbances," *IEEE Journal of Emerging and Selected Topics in Power Electronics*, vol. 10, no. 1, pp. 413-423, Feb. 2022.

[15] S. Ghosh, M. K. Bakhshizadeh, G. Yang *et al*., "Nonlinear stability investigation of type-4 wind turbines with non-autonomous behavior based on transient damping characteristics," *IEEE Access*, vol. 11, pp. 76059-76070, Jul. 2023.

[16] J. W. Baker, "Stability properties of a second order damped and forced nonlinear differential equation," *SIAM Journal on Applied Mathematics*, vol. 27, no. 1, pp. 159-166, Jul. 1974.

[17] S. Izumi, H. Somekawa, X. Xin *et al*., "Estimation of regions of attraction of power systems by using sum of squares programming," *Electrical Engineering*, vol. 100, no. 4, pp. 2205-2216, May 2018.

[18] B. Wang, B. Fang, Y. Wang *et al*., "Power system transient stability assessment based on big data and the core vector machine," *IEEE Transactions on Smart Grid*, vol. 7, no. 5, pp. 2561-2570, Sept. 2016.

[19] G. Contessa, "Scientific models and fictional objects," *Synthese*, vol. 172, no. 2, p. 215, Mar. 2009.

[20] R. A. Nelson and M. G. Olsson, "The pendulum-rich physics from a simple system," *American Journal of Physics*, vol. 54, no. 2, pp. 112-121, Feb. 1986.

[21] K. Furuta and M. Iwase, "Swing-up time analysis of pendulum," *Bulletin of the Polish Academy of Sciences*, *Technical Sciences*, vol. 52, no. 3, pp. 153-163, Dec. 2004.

[22] G. D. Birkhoff, "The restricted problem of three bodies," *Rendiconti Del Circolo Matematico Di Palermo* (*1884-1940*), vol. 39, no. 1, pp. 265-334, Dec. 1915.

[23] B. Bläsi and L. Hardy, "Realism and time symmetry in quantum mechanics," *Physics Letters A*, vol. 207, no. 3-4, pp. 119-125, Oct. 1995.

[24] Y. Aharonov and J. Tollaksen. (2007, Jun.). New insights on time-symmetry in quantum mechanics. [Online]. Available: http://arXiv: 0706. 1232.2007

[25] S. E. Vlad, *Boolean Functions: Topics in Asynchronicity*, 1st ed. New York: Wiley, 2019.

[26] J. S. W. Lamb and J. A. G. Roberts, "Time-reversal symmetry in dynamical systems: a survey," *Physica D*: *Nonlinear Phenomena*, vol. 112, no. 1-2, pp. 1-39, Jan. 1998.

[27] S. Ghosh, M. K. Bakhshizadeh, G. Yang *et al*., "Non-linear stability boundary assessment of offshore wind power plants under large grid disturbances" in *Proceedings of 21st Wind & Solar Integration Workshop* (*WIW 2022*), Hague, The Netherlands, Oct. 2022, pp. 1-9.

[28] M. K. Bakhshizadeh, S. Ghosh, Ł. Kocewiak *et al*., "Improved reduced-order model for PLL instability investigations," *IEEE Access*, vol. 11, pp. 72400-72408, Jul. 2023.

[29] H. K. Khalil, *Nonlinear Systems*, 2nd ed. New Jersey: Prentice Hall, 2002.

[30] Mathonline. (2022, Nov.). The boundary of a set under homeomorphisms on topological spaces. [Online]. Available: http://mathonline. wikidot. com/the-boundary-of-a-set-under-homeomorphisms-on-topological-sp

[31] J. A. G. Roberts and G. R. W. Quispel, "Chaos and time-reversal symmetry. Order and chaos in reversible dynamical systems," *Physics Reports*, vol. 216, no. 2-3, pp. 63-177, Jul. 1992.

[32] R. Genesio, M. Tartaglia, and A. Vicino, "On the estimation of asymptotic stability regions: state of the art and new proposals," *IEEE Transactions on Automatic Control*, vol. 30, no. 8, pp. 747-755, Aug. 1985.

[33] TenneT TSO GmbH, "Offshore-Netzanschlussregeln (O-NAR)," Tech. Rep., Aug. 2019.

[34] Ł. Kocewiak, Y. Sun, B.-G. Ramon *et al*., "Overview, status and outline of stability analysis in converter-based power systems," in the *Proceedings of the 19th International Workshop on Large-scale Integration of Wind Power into Power Systems as well as Transmission Networks for Offshore Wind Farms*, Ljubljana, Slovenia, Jan. 2020, pp. 1-10.

[35] M. G. Taul, X. Wang, P. Davari *et al*., "Reduced-order and aggregated modeling of large-signal synchronization stability for multiconverter systems," *IEEE Journal of Emerging and Selected Topics in Power Electronics*, vol. 9, no. 3, pp. 3150-3165, Jun. 2021.

[36] H. Wu and X. Wang, "Design-oriented transient stability analysis of grid-connected converters with power synchronization control," *IEEE Transactions on Industrial Electronics*, vol. 66, no. 8, pp. 6473-6482,

Aug. 2019.

Mohammad Kazem Bakhshizadeh received the B.S. and M.S. degrees in electrical engineering from Amirkabir University of Technology, Tehran, Iran, in 2008 and 2011, respectively, and the Ph. D. degree from Aalborg University, Aalborg, Denmark, in 2018. In 2016, he was a Visiting Scholar at Imperial College London, London, U.K.. He is currently a Senior Power System Engineer at Ørsted Wind Power, Fredericia, Denmark. His research interests include power quality, modelling, control and stability analysis of power converters, and grid converters for renewable energy systems.

Sujay Ghosh received the M. Sc. degree in electrical engineering from the Technical University of Denmark (DTU), Kgs. Lyngby, Denmark, in 2019. Currently, he is a Ph. D. candidate at Ørsted Wind Power A/S, Gentofte, Denmark, pursuing his Ph.D. degree on the stability of large renewable power plants in low inertia systems, in association with DTU. Previously, he has also worked as a system studies engineer in the electrical industry in India and Denmark. His research field is in power system stability and control.

Guangya Yang joined the Technical University of Denmark (DTU), Kgs. Lyngby, Denmark, in 2009, and is currently a Senior Scientist with the Department of Wind and Energy Systems. Previously, he has also been a full-time employee at Ørsted Wind Power A/S, Gentofte, Denmark, working on the electrical design of large offshore wind farms. He has received numerous research grants, including the recent H2020 MSCA ITN project InnoCyPES as coordinator. He is currently serving as Lead Editor for IEEE Access Power and Energy Society Section and has been an editorial board member of several journals. He is a member of the IEC Technical Committee "Wind Power Generation Systems" (TC88) and the convenor of IEC 61400-21-5. His research field is in stability, control, and operation of power systems.

Łukasz Kocewiak received the B.Sc. and M.Sc. degrees in electrical engineering from Warsaw University of Technology, Warsaw, Poland, in 2007, as well as the Ph.D. degree from Aalborg University, Aalborg, Denmark, in 2012. Currently, he is with Ørsted Wind Power A/S, Gentofte, Denmark and is working as an R&D Manager. He is a power system specialist in the area of design of electrical infrastructure in large offshore wind power plants. The main direction of his research is related to harmonics, stability, and nonlinear dynamics in power electronics and power systems especially focused on wind power generation units.